An effective method to probe local magnetostatic properties in a nanometric FePd antidot array

2011 New J. Phys. 13 013035

(http://iopscience.iop.org/1367-2630/13/1/013035)

New Journal of Physics
The open-access journal for physics

An effective method to probe local magnetostatic properties in a nanometric FePd antidot array

F Béron[1,3], K R Pirota[1], V Vega[2], V M Prida[2], A Fernández[2], B Hernando[2] and M Knobel[1]

[1] Instituto de Física Gleb Wataghin, Universidade Estadual de Campinas, Rua Sergio Buarque de Holanda, 777, Cidade Universitária 'Zeferino Vaz', Campinas 13083-859, SP, Brazil

[2] Depto. Física, Universidad de Oviedo, Calvo Sotelo s/n, 33007 Oviedo, Asturias, Spain

E-mail: fberon@ifi.unicamp.br

New Journal of Physics **13** (2011) 013035 (16pp)
Received 16 August 2010
Published 25 January 2011
Online at http://www.njp.org/
doi:10.1088/1367-2630/13/1/013035

Abstract. A simple method to quantitatively characterize the local magnetic behaviour of a patterned nanostructure, like a ferromagnetic thin film of antidot arrays, is proposed. The first-order reversal curve (FORC) analysis, coupled with simulations using physically meaningful hysterons, allows us to obtain a quantitative and physically related description of the interaction field and each magnetization reversal process. The hysterons system is built from previously known hypotheses on the magnetic behaviour of the sample. This method was successfully applied to a highly hexagonal ordered FePd antidot array with nanometric dimensions. We achieved a complete characterization of the two different magnetization reversal mechanisms in function of the in-plane applied field angle. For a narrow range of high fields, the magnetization initiates rotating reversibly around the pores, while at lower fields, domain walls are nucleated and propagated. This in-plane magnetization reversal mechanism, partly reversible and partly irreversible, is the only angularly dependent one. While going away from the easy axis, its reversible proportion increases, as well as its switching field distribution. Finally, the results indicate that the high surface roughness between adjacent holes of the antidot thin film induces a parallel interaction field. The proposed method demonstrates its ability also to be applied to characterizing patterned nanostructures with rather complex magnetization reversal processes.

[3] Author to whom any correspondence should be addressed.

Contents

1. Introduction

The magnetic behaviour of antidot arrays (thin films with a mesh of embedded patterned holes) strongly differs from that of the continuous film counterparts, owing to the competition between the intrinsic thin film anisotropy and the shape anisotropy induced by the holes themselves, thus altering the demagnetizing fields. Their magnetization reversal, mainly governed by nucleation and propagation of domain walls, can be controlled by means of the holes' geometrical arrangement (size, lattice parameter and spatial symmetry ordering), which can act as pinning centres hindering the domain wall propagation [1, 2]. These features yield to the possible tailoring of magnetic properties such as magnetoresistance, coercive field, anisotropy and permeability [3]–[6]. Also, owing to their well-controlled nanoscale pattern, antidot arrays were successfully used as an ideal system in order to test theoretical models describing vortex pinning in superconductors, for example [7, 8]. The lack of the superparamagnetic limit, once the system does not contain small isolated magnetic entities, is appealing for high-density information storage and magneto-optical applications [9, 10]. Very recently, the new and interesting use of antidot arrays as magnonic crystals has been proposed [11]. Similar to photonic crystals (for light), the magnonic crystals are expected to provide full control of spin waves. This could contribute to develop novel high-speed data transfer rate devices, as a promising way to transmit information without moving electron charges [12].

Taking into account all of the above-mentioned potential uses, further control and understanding of the magnetic properties of this rather new material, including the magnetization reversal mechanisms, appear to be a very important task. The key point lies in the overall effect that comes from the local modulation of the magnetization, which is induced by the presence of holes in the film. The most common magnetometry experiments only allow one to evaluate the macroscopic magnetic properties, while local probe techniques (such as magnetic force microscopy, magneto-optical Kerr effect and x-ray magnetic circular dichroism) generally involve expensive and dedicated equipment, complexity in sample preparation or a very limited

probed area. Here, we propose a rather simple magnetostatic method that allows one to obtain not only the magnetization reversal processes, but also important quantitative information (switching field, interaction field, etc) about the local magnetic behaviour of nanometric antidot arrays.

The proposed method is based on the first-order reversal curve (FORC) technique [13], which has already proved its efficiency to characterize systems consisting of magnetic entities (i.e. array of nanodots [14, 15], nanopillars [16] and nanowires [17]–[20], among others). A recent attempt was made to use the FORC method to characterize patterned thin films [21]. However, accurate quantitative analysis of the results is rather difficult, especially for systems exhibiting a complex magnetization reversal process. In these cases, a direct quantitative analysis of the FORC distribution usually turns out to be inexact, because the system behaviour diverges from the FORC technique mathematical basis, which is the classical Preisach model [22]. As an alternative, we suggest using the physical analysis model in order to simulate the experimental FORC result [23]. The physical accuracy of the simulation is guaranteed by the concordance with others means of characterization, such as micromagnetic simulations and microstructural characterization, which give insights into the possible experimental behaviour of the system. This procedure allows one to obtain accurate quantitative values of each local magnetostatic property of systems with complex magnetization reversal.

In this work, we focus on the characterization of a typical nanometric antidot array exhibiting field-induced anisotropy. It consists of an FePd thin film deposited on the top surface of a highly hexagonal-ordered nanoporous alumina template. The high pore length/diameter ratio ($4\,\mu$m/35 nm) prevents most of the magnetic material from entering the pores. The as-obtained structure is expected to exhibit a magnetization reversal by nucleation–propagation of domain walls [1]. Instead of extracting directly the antidot magnetostatic properties from the experimental FORC result, the proposed procedure based on the physical analysis model was successfully applied to different field angles, keeping the applied field in-plane. This led to a complete characterization of its local magnetic behaviour.

2. First-order reversal curve (FORC) procedure

The FORC method represents an effective way of probing the local magnetostatic properties of a nanostructure [14]–[20]. Despite the fact that the analysis of results is more intuitive for systems constituting single-domain magnetic entities, it can still be successfully applied to structures having a more complex magnetization reversal behaviour. After reversing the applied field direction, the change of magnetization M is only proportional to the fraction of pure irreversible processes (represented by a square hysteresis loop with a coercivity H_c and a bias field H_u, called 'mathematical hysteron') that returned to their initial state. The generalization of this concept leads to the FORC distribution function ρ, which represents the statistical distribution of the mathematical hysterons. With H as the applied field and H_r as the reversal field, ρ is defined as

$$\rho(H, H_r) = -\frac{1}{2}\frac{\partial^2 M(H, H_r)}{\partial H \partial H_r} \quad (H \geqslant H_r), \tag{1}$$

when multiple minor loops, called FORCs, are measured from different values of the reversal field until the positive saturation (inset of figure 1) [13]. The calculated FORC distribution,

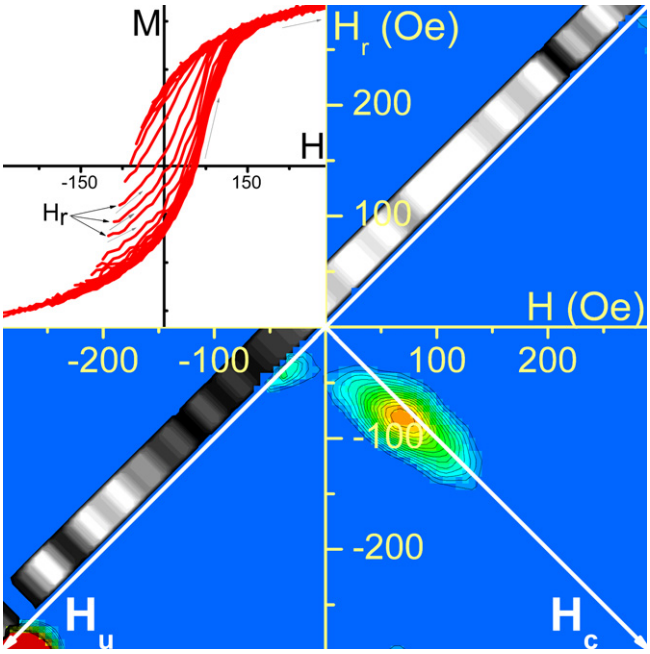

Figure 1. FORC result from the analysis of minor hysteresis loops shown in the inset. (27 nm-thick $Fe_{73}Pd_{27}$ continuous thin film, in-plane applied field 60° away from its easy axis).

which is only related to the irreversible processes, is represented as a contour plot, ranging from blue to red for positive values of ρ while it varies from blue to black for negative values of ρ (figure 1). It is called an extrapolated FORC diagram when the $H < H_r$ region is filled with extrapolated data points, in a way that minimizes the M derivative at $H = H_r$. This procedure allows one to avoid the influence of the presence of reversible processes of magnetization in the quasi-reversible region ($H_c \approx 0$ Oe) [24]. The precision of the result is governed by the magnetic field and reversal field steps, ΔH and ΔH_r, respectively [20]. It is usually analysed by employing the interaction field axis [$H_u = -(H + H_r)/2$] and the critical field axis [$H_c = (H - H_r)/2$]. An estimation of the reversible processes' contribution can be achieved through the susceptibility ratio of the major hysteresis curve and the FORCs at each reversal fields, called the reversibility indicator [24]. This result is depicted as a greyscale strip line ranging from black (0% reversible) to white (100% reversible) [20].

Like most physical systems, the FORC result cannot be interpreted by the classical Preisach model, because the antidot array behaviour violates the congruency principle [13]. However, by combining the results obtained from other characterization techniques with the FORC method, we can describe our system by physically meaningful hysterons and compare the simulated FORC diagrams with the experimental ones (see [23]). This procedure allows one to achieve an accurate and physically related quantitative characterization of the reversible and irreversible magnetic behaviour of the studied system.

The first step consists of examining the FORC result in order to gain global insights into the magnetic behaviour of the sample. Even if the FORC distribution only represents direct information about magnetization irreversible processes, it is also influenced by the reversible ones in the presence of a non-static interaction field, such as a mean interaction field [20].

Consequently, the FORC diagram should be considered as a complete representation of the magnetization reversal behaviour. For the irreversible contribution, it is needed to consider both the interaction field and switching field effects together.

The second step of the analysis involves gathering the maximum of information about the microstructure and magnetostatic properties of the real sample, in order to relate them to physical processes and features. This helps to elaborate an accurate model of physical hysterons that is used afterwards to simulate the FORC diagram. It can be achieved through any adequate technique, theoretical or experimental, that will give meaningful insights into the system behaviour. For the FePd antidot film, we performed microstructural characterization by means of scanning and transmission electron microscopy techniques (SEM and TEM) and x-ray diffraction (XRD), together with atomic force microscopy (AFM) to characterize the film surface roughness and micromagnetic simulations of a flat antidot film.

3. Antidot experimental details

3.1. Fabrication

A highly hexagonal-ordered array of $Fe_{73}Pd_{27}$ antidot film (interpore distance $D = 105$ nm, diameter $d = 35$ nm and thickness $t = 47$ nm) was fabricated by controlled deposition of the metallic alloy on a patterned template employing a vacuum thermal evaporation technique [25]. The two pure metal targets were thermally evaporated on the top surface of a hexagonally ordered nanoporous alumina membrane with a honeycomb-like structure, used as a template [26], which was previously synthesized by following a well-known two-step anodization procedure in oxalic acid, as reported elsewhere [27, 28]. The deposition process was carried out in a high-vacuum system (4×10^{-6} mbar), having a diffusion pump backed by rotary pumping together with a liquid nitrogen trap. A radiant heater, coupled to a temperature controller, was employed in order to maintain the substrate temperature in the range of $20 \pm 2\,^{\circ}$C. The source to substrate distances were maintained at about 18 cm, in order to get a low and constant deposition rate of around 0.1–0.15 nm s^{-1}. The antidot film growth was monitored through a quartz crystal thickness.

3.2. Film characterization

The top-view SEM image of the FePd antidot thin film is shown in figure 2(a), displaying the highly hexagonal ordering of antidots having a hole mean diameter around 35 and 105 nm of the lattice parameter. The inset shown below displays the high-magnification figure of one single antidot, where the holes appear in dark grey and the crests formed by the surface roughness in light grey. In addition to the expected holes, the obtained film surface presents a regular roughness, being the material deposition preponderant between the holes' intersection surface of the alumina template (figure 2(a)).

Energy-dispersive x-ray (EDX) spectroscopy shows that the deposited material is effectively composed of Fe and Pd (figure 2(b)). The presence of Al and O from the alumina substrate was also detected. The analysis of the spectrum leads to an Fe/Pd ratio of 73 : 27. This ratio was carefully chosen in order to obtain an alloy exhibiting the magnetic shape memory effect (see [29] and references therein). Indeed, for continuous thin film grown under identical conditions, a uniaxial anisotropy direction (easy axis) was created along the first applied

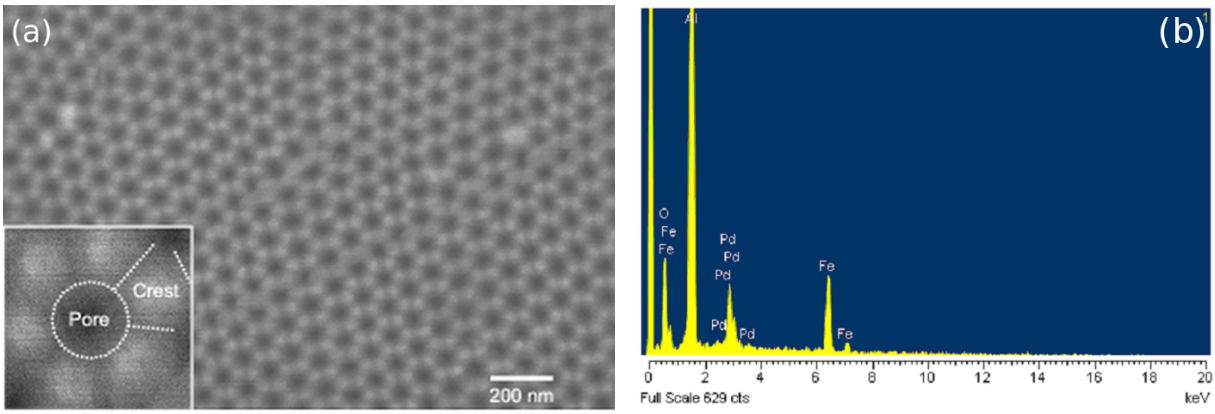

Figure 2. (a) SEM top-view image of the $Fe_{73}Pd_{27}$ thin film antidot array surface. Inset displays a high-magnification image of a single antidot. (b) EDX analysis with SEM, showing the Fe and Pd content of the antidot array (O and Al belong to the alumina template substrate).

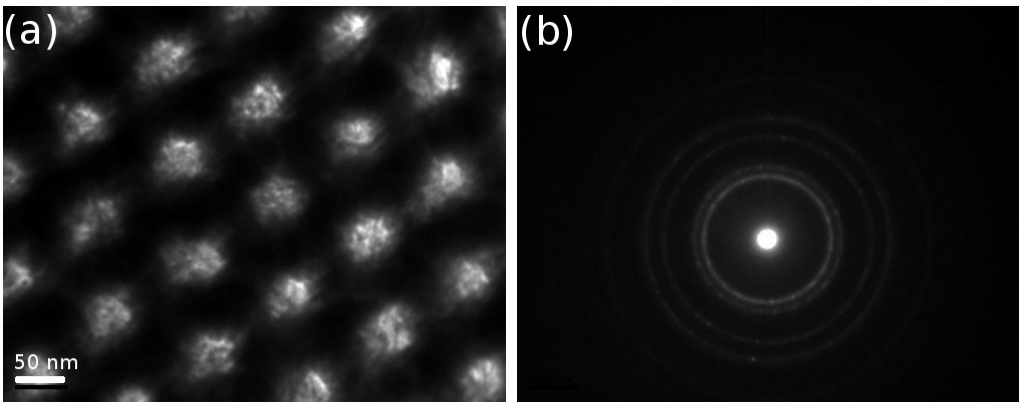

Figure 3. (a) TEM image of as-deposited $Fe_{73}Pd_{27}$ antidots thin film (b) corresponding SAED pattern exhibiting its polycrystalline nature.

magnetic field orientation. This anisotropy remains during the time range of the measurements, despite application of high magnetic fields along other orientations.

Finally, figure 3(a) shows the representative TEM image of as-deposited FePd antidot thin film after removing the substrate of the alumina template by chemical etching in NaOH solution. It displays the highly hexagonal ordering of the antidots. The corresponding selected area electron diffraction (SAED) pattern shown in figure 3(b) clearly reveals that the as-deposited FePd film is polycrystalline.

3.3. Surface characterization

We investigated the height elevation of the FePd antidot film surface by AFM. The main objective pursued by this characterization was to measure the height of the crests produced at the film surface. Figures 4(a) and (b) present typical top-view AFM images of surfaces with $1\ \mu m \times 1\ \mu m$ area of, respectively, the clean alumina template (without film deposition) and

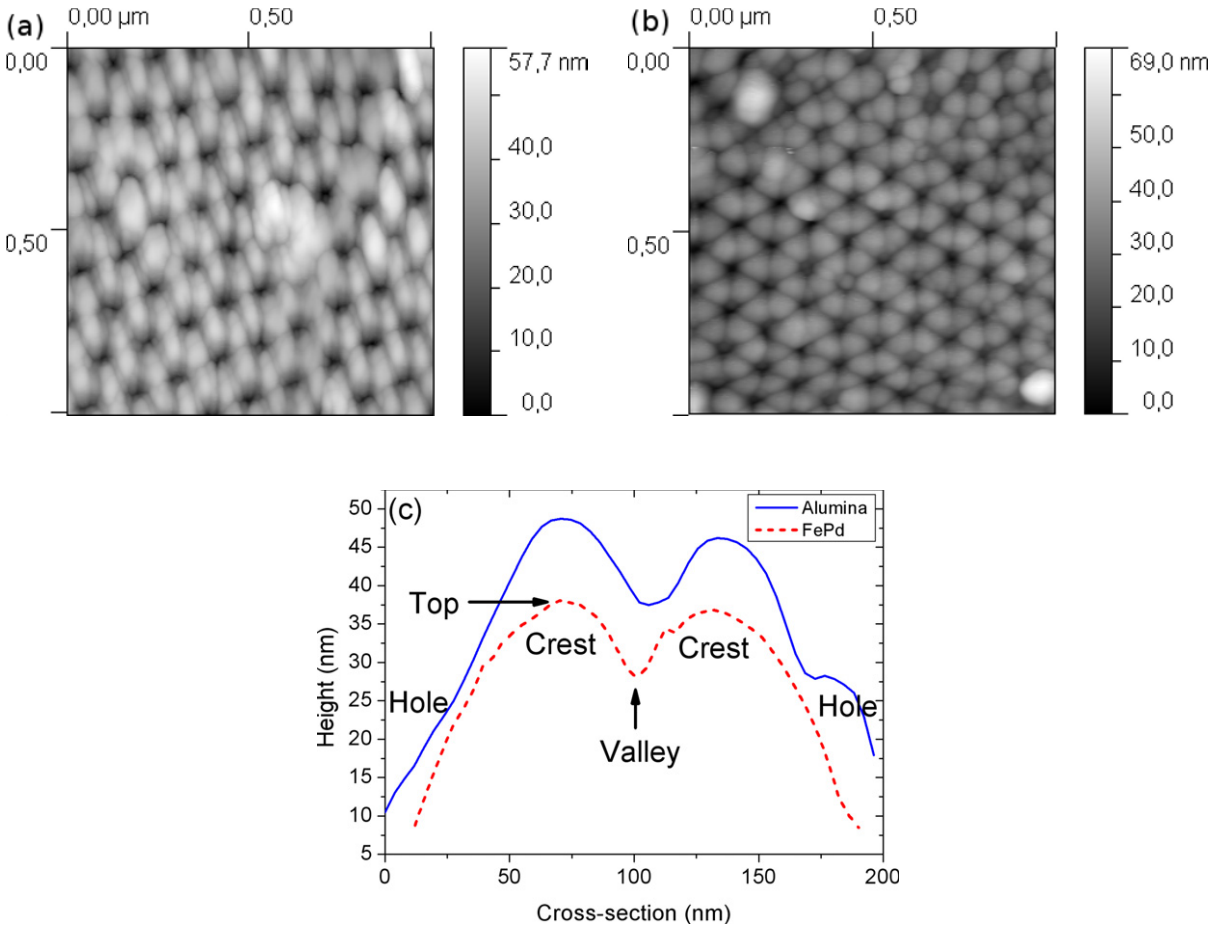

Figure 4. Top view of a 1 μm $\times$ 1 μm AFM scan of (a) the clean alumina surface (b) the antidot film surface and (c) an AFM scan cross-section between two neighbour pores, in order to measure the crest height.

the FePd antidot thin film after being deposited onto the surface of the alumina template. On both images, the regular crest pattern is clearly visible, standing at each intersection between pores, as was observed on the SEM image in the antidot case (see figure 2(a)). The crest height determination was executed by measuring the height difference between the top and the valley created at the surface, when drawing a cross-section between two adjacent pores (figure 4(c)). A conical AFM tip was used in order to limit the artefacts due to the tip shape. This procedure was repeated around 50 times at different regions of the scanned area. The average crest height values were found to be similar with (9 ± 4 nm) and without (8 ± 3 nm) the antidot thin film, showing that the thin film follows the alumina surface. Therefore, it is worth noting that the observed roughness of the antidot film surface comes from the fabrication process of the nanoporous alumina template. During the second anodization stage, the alumina grows by replicating the aluminium surface, which was previously patterned by the first anodization process, leading to the regular pattern observed [28].

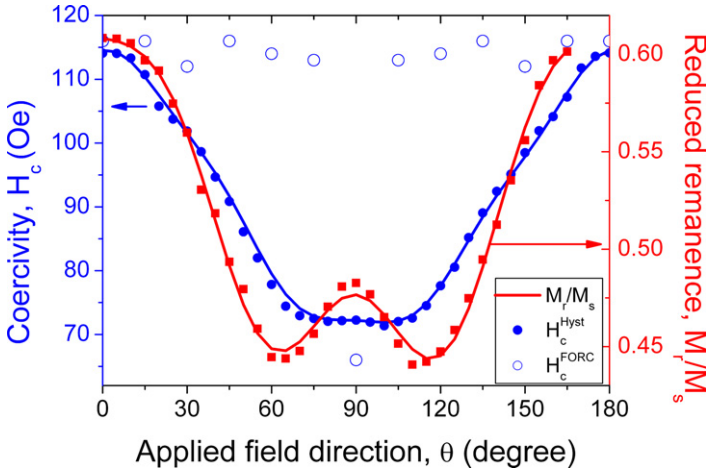

Figure 5. Influence of the in-plane applied field angle θ on the coercivity and the reduced remanence. The experimental data (points) of the global properties were well fitted with equation (2) (lines).

4. Experimental application of the procedure

4.1. Angular dependence of global properties

Small-angle x-ray scattering (SAXS) performed at the Laboratorio Nacional de Luz Sincroton (LNLS), Campinas, Brazil, showed that, despite the hexagonal short-range hole order, the antidot array does not sustain long-range hole ordering on the whole sample. This can be explained by the fact that the hole-ordered regions form domains aligned towards different directions, as can be seen in figure 2(a). Nevertheless, measurements of the global magnetostatic properties, via major hysteresis curves, exhibit strong angular dependence while keeping the applied field in-plane. Both the global coercivity (H_c^{Hyst}) and the reduced remanence (M_r/M_s) present near-uniaxial anisotropic behaviour, as can be observed in figure 5. Due to the periodicity exhibited by both curves, a phenomenological expression based on *cos* terms of their angular behaviour was constructed. Each best fit of the lowest periodicity *cos* term was subtracted one after another from the remaining curve, until reaching the noise level. By proceeding in this way, experimental data were accurately fitted with the expression

$$P\cos(2\theta) + Q\cos(4\theta) + R\cos(6\theta) + S\cos(8\theta), \tag{2}$$

where θ represents the angle between the in-plane applied field and the effective easy axis of the antidot array. This cannot be related to a specific direction of the hexagonal short-range hole order, due to the lack of long-range order of the antidot array. Interestingly, even if the predominant behaviour is similar for the global coercivity and the reduced remanence, they are not identical, giving different fit coefficient values. Both represent global properties, which can depend on several different factors. Reflecting the predominantly in-plane uniaxial behaviour, the coefficient P is the largest, followed by Q (88–7% and 66–21% for respectively H_c^{Hyst} and M_r). Only M_r presents a sixfold anisotropy axis ($R = 13\%$), whereas H_c^{Hyst} exhibits instead an eightfold one ($S = 5\%$). Therefore, the FePd uniaxial anisotropy (as measured on a plain thin film) seems to be the main contribution to the antidot array effective anisotropy. Only a small

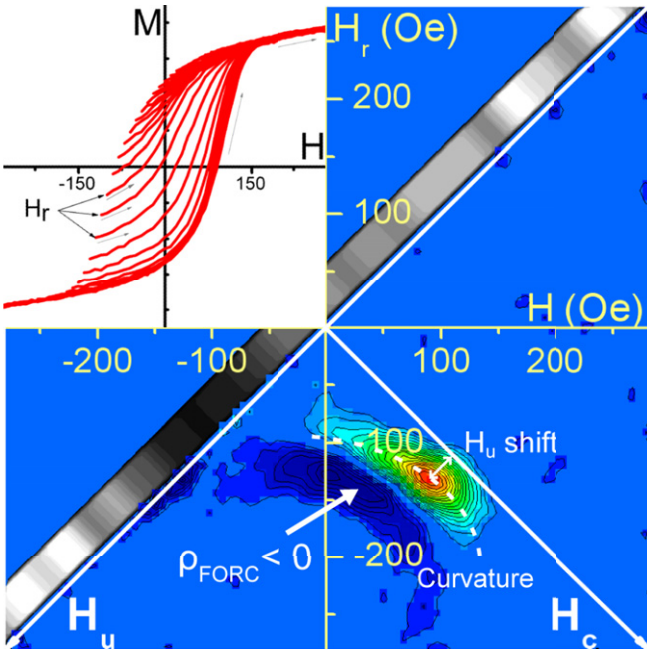

Figure 6. Typical experimental in-plane-extrapolated FORC result of a nanometric-ordered antidot array (FORCs curves are shown in the inset). ($Fe_{73}Pd_{27}$, $\theta = 60^\circ$, $d = 35$ nm, $D = 105$ nm, $t = 47$ nm).

proportion of the remanence angular behaviour can be associated with the hexagonal short-range ordering of the holes.

4.2. FORC characterization

Figure 6 shows the measured representative experimental FORC diagram of the nanometric hexagonal-ordered FePd antidot array. The magnetic field was applied parallel to the sample plane, with a constant and equal value of 10 Oe for both the magnetic field and reversal field's increment steps, and up to a saturation field of 10 kOe. Measurements were carried out at room temperature on a commercial vibrating sample magnetometer (VSM).

The non-null susceptibility of the FORCs at the reversal field, leading to a grey indication of the reversibility, indicates that contribution to the magnetization reversal occurs by reversible processes. The reversibility indicator value related to the FORC distribution maximum ($H_r = 130$ Oe) gives a proportion of around 65%. The FORC diagram exhibits two distributions: one positive and one negative. Both are elongated along the coercivity axis. These features suggest the presence of a broad switching field distribution under the presence of a parallel mean interaction field ($H_{int} = kM$, with $k > 0$). Indeed, while the addition of a parallel mean interaction field to a monodisperse irreversible system translates the Dirac peak of the FORC distribution towards higher values on the H_c-axis [23], the consequences change drastically for a system having a large switching field distribution. Generally speaking, the interaction field could modify the FORC distribution curvature, slightly shifting it towards positive H_u values and inducing a negative region beneath the positive distribution [30]. All three features are clearly visible on the experimental FORC diagram shown in figure 6. Briefly, the experimental

FORC result analysis suggests that the antidot array local magnetic behaviour consists of a mixture of reversible and distributed irreversible magnetization processes being submitted to a parallel interaction field. From the comparison with the FORC result of a continuous thin film deposited and measured under the same conditions (figure 1), it appears that the hole presence induces the parallel interaction field, as well as increases the local coercivity (75 versus 115 Oe).

4.3. Micromagnetic simulations

We performed micromagnetic simulations, with the help of the OOMMF software[4], in order to investigate the magnetization reversal processes of the hexagonal-ordered antidot array, neglecting the film surface roughness. The clear interconnection between the pillars shown in figure 2(a) allows this approximation for a qualitative interpretation. We previously determined the magnetic material parameters from the characterization of an FePd thin film grown under identical conditions as those for the antidot array. The saturation magnetization was measured with a VSM ($M_s = 2.5 \times 10^6\,\mathrm{A\,m^{-1}}$). Ferromagnetic resonance, measured as a function of the in-plane applied field angle, was used to get the effective anisotropy constant ($K = 19\,375\,\mathrm{J\,m^{-3}}$). Finally, the exchange stiffness constant was extracted from the temperature dependence of saturation magnetization by Bloch's law ($A = 1.05 \times 10^{-12}\,\mathrm{J\,m^{-1}}$). In order to mimic exactly the hole ordering of the FePd antidot array sample, instead of a perfect arrangement, a two-coloured $2.1\,\mu\mathrm{m} \times 1.45\,\mu\mathrm{m}$ SEM picture was used as a mask to delimit the magnetic material, with a square unit cell of 5 nm. The hole diameter was adjusted to 35 nm during this greyscale to black and white transformation.

The simulated remanent domain pattern after a saturation along the easy axis, as defined by the anisotropy constant ($\theta = 0^\circ$), exhibits two different behaviours (figure 7(a)). The shape anisotropy induces the rotation of the magnetization around the holes, which can be seen from the alternation of black and coloured regions. This rotation is the first magnetization reversal process that occurs when the applied magnetic field is reduced from saturation and can be associated with the reversible contribution to the magnetization reversal found from the FORC curves. In addition, some areas, which are delimited by holes that act as pinning sites, already have their magnetization reversed and therefore appear in red instead of blue. These magnetic domains appear and grow abruptly, mainly in regions presenting large interpore distance along the applied field direction. This nucleation process accounts for irreversible switching. Simulations performed with applied field not aligned parallel to the uniaxial effective anisotropy of the film ($\theta \neq 0^\circ$) show that the domain wall propagation continuously occurs along the anisotropy direction.

Figure 7(b) presents a typical simulated hysteresis curve, compared with the experimental measured one (both acquired along the $\theta = 60^\circ$ direction). The good agreement between experimental and simulated global coercivity ($H_c \approx 80$ Oe) leads to the above conclusions about the hole pattern structural induced magnetization reversal processes really reliable. It is worth noting, however, the discrepancy exhibited by the susceptibility χ at zero field. A parallel mean interaction field of 850 Oe has to be added to the simulated hysteresis curve in order to achieve the same susceptibility. This disparity suggests that the film surface roughness of the antidot array, which is the main difference between the simulated and measured antidot sample, could

[4] The 'Object Oriented Micromagnetic Framework,' developed at NIST, Gaithersburg—http://math.nist.gov/oommf/.

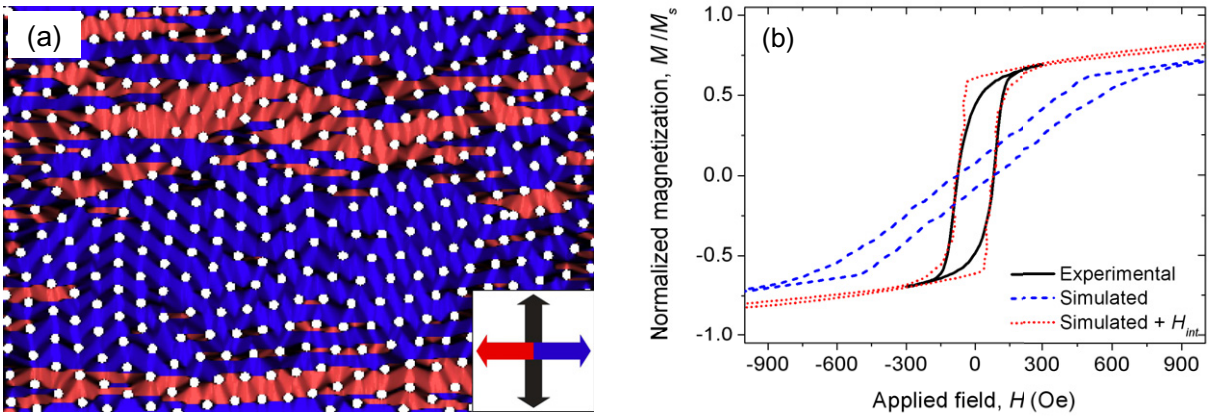

Figure 7. Micromagnetic simulation results: (a) simulated magnetic domain pattern of the antidot array in the remanent state, after applying a magnetic field towards the right direction (easy-axis direction). Spins pointing to the right appear in blue, to the left in red and vertically in black, respectively. (b) Experimental (solid), simulated (dashed) and simulated with an additional parallel mean interaction field of 850 Oe (dotted) major hysteresis curves ($\theta = 60^{\circ}$).

lead to a dipolar interaction field along the magnetization direction, an assumption strengthened by the absence of a parallel interaction field visible on the continuous thin film FORC result (see figure 1). Another visible discrepancy is the saturation approach, which is much smoother in the experimental case. This could be related to the non-uniformity of the film surface roughness, which in turn leads to a non-uniformity of the dipolar interaction field along the magnetic antidot array. Therefore, the value used for the mean interaction field (850 Oe) should not be considered as an estimation of the real average value of the interaction field. Moreover, other differences existing between the systems compared (different areas, border effects, etc.) could seriously influence the interaction field.

4.4. Simulated FORC result

The previous micromagnetic simulations revealed two main magnetization reversal processes: one of reversible character, concerning the magnetization rotation around the holes, and another irreversible, due to the magnetic domain formation and growth. Each process was depicted by a physical hysteron representing a first approximation of their magnetic behaviour, which can be characterized by its saturation field H_{A} (figure 8). A reversible hysteron, with identical saturation value to the irreversible one, was added to the domain wall nucleation–propagation process in order to account for the possible difference between the applied field and effective anisotropy direction. For similar reasons, a broad distribution was imposed on the switching field value of the irreversible hysteron. The simulated system was completed with the features of the antidot film surface roughness, namely a distributed interaction field H_{int}, parallel to the magnetization, mimicking the role played by the dipolar interactions between the sample surface crests. The initial values were estimated from the previous magnetic characterizations, all distributions taken as Gaussian.

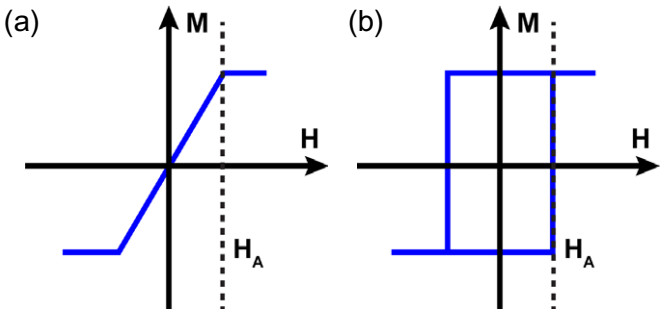

Figure 8. Shape of (a) reversible and (b) irreversible physical hysterons used for the simulation with the physical analysis model. Both are characterized by their respective saturation field H_A.

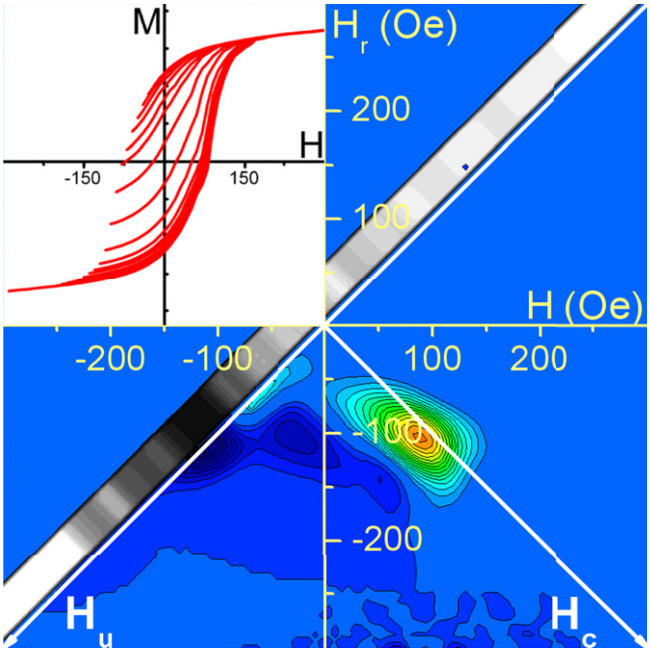

Figure 9. Simulated extrapolated FORC diagram with the physical analysis model (FORCs curves are shown in the inset).

Figure 9 presents the best fit obtained by adjusting the various parameters of the simulated system (see table 1 for the optimized values). Considering the fact that quantitative analysis must be carefully made, because different systems can exhibit identical FORC diagrams [23], the system complexity and good agreement exhibited between the FORC distributions favour the hypothesis that the simulated system adequately represents the local magnetic behaviour of the antidot array film.

The proposed procedure of FORC analysis appears to be the unique way of obtaining the exact values of local magnetostatic properties (switching field, magnetization rotation, dipolar field, etc), especially the distribution broadness. According to these results, most of the sample's magnetization reversal occurs by means of reversible processes. The fitted value of 65% agrees well with the one previously found through the reversibility indicator calculation.

Table 1. Description of the local magnetic behaviour of the nanometric antidot array (and the continuous thin film for comparison, in parentheses) with the physical analysis model (optimized values). All distributions are Gaussian.

Physical process	Model representation	Characteristic (Oe) (H_A or k)	Proportion (%)
Magnetization rotation	Reversible hysterons	1500 ± 10	40%
Domain wall nucleation–propagation	Irreversible hysterons	115 ± 45 (75 ± 25)	35% (50%)
Domain wall nucleation–propagation	Reversible hysterons	115 ± 100 (75 ± 100)	25% (50%)
Dipolar field	Mean interaction field ($H_{int} = kM$)	100 ± 30	–

In comparison, the magnetization reversal of the continuous thin film presented in figure 1 occurs only by domain wall nucleation–propagation, with a smaller switching field. The discrepancy between the coercivity measured on the major hysteresis curve and the switching field fitted value (80 versus 115 Oe) must also be pointed out. However, both values do not represent physically the same situation; the hysteresis curve gives a global indication while the FORC is related to the local magnetic behaviour. Thereby, from an application point of view, it is important to easily obtain access to both behaviours. This will help to adequately design the nanostructure in order to meet the application specifications.

One remarkable feature of the physical analysis model applied to FORC results remains in its ability to quickly reproduce a complex hysteretic behaviour with simple entities, the so-called physical hysterons. Indeed, the domain wall nucleation and propagation are processes where the magnetic entity properties, such as the switching field, change during magnetization reversal. However, the simulated system, which consists of a static irreversible distribution, still yields to an adequate magnetic characterization of this rather complex nanostructure.

4.5. Angular dependence of local properties

This situation represents a typical example where the tool of the physical analysis model, after measuring the FORCs of the sample, is revealed to be highly interesting from a characterization point of view. While the global magnetostatic properties extracted from the major hysteresis curves only give an indication of the average magnetization of the antidot, the physical analysis model permits one to discriminate between each magnetization reversal process and to follow the influence of a given parameter (here, the applied field direction) on the local properties. Using the results presented in table 1, we fitted the FORC distributions measured for different in-plane field angles (θ). As a first approximation, the values concerning the magnetization rotation and the dipolar field were kept constant because, depending on the shape anisotropy induced by the holes and the crests at the film surface, an angular dependence is not expected. Figure 4 shows that the local coercivity (H_c^{FORC}), taken as the H_c coordinate of the FORC distribution maximum, remains constant ($\sim$115 Oe) until a sudden drop at $\theta = 90^\circ$, instead of following the global coercivity trend. Therefore, the mean value of the domain wall nucleation field, the only irreversible process, was also fixed at 115 Oe (no fit was achieved at 90° with a smaller domain wall nucleation field).

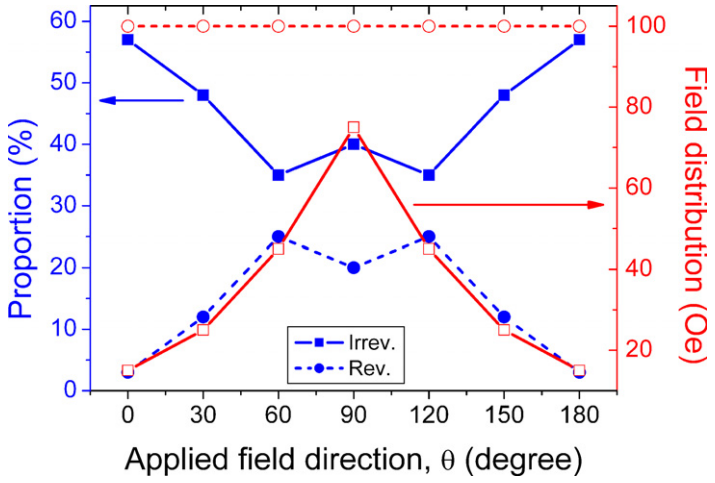

Figure 10. Influence of the in-plane-applied field angle θ on the fitted parameters for the domain wall nucleation–propagation process (irreversible (square) and reversible (circle) hysterons), according to the physical analysis model.

Figure 10 presents the fitted values for the reversible and irreversible hysterons associated with the domain wall nucleation–propagation process, the only one influenced by the applied field direction. While passing from the easy axis (0°) to the hard axis (90°), the irreversible proportion decreases before increasing a little. It is worth remarking that it follows the same trend as the remanence, the domain wall nucleation being the only irreversible process. The small disparity between the values (around 10%) can be attributed to two main points: (i) the M_r value is highly dependent of the maximum field applied, especially in the present case where the system slowly saturates at the high field (more than 1500 Oe); and (ii) the parallel interaction field can contribute to the remanence, but will not affect the irreversible proportion. Therefore, the physical analysis model of the angular FORC diagrams shows that the angular dependence of the remanence is directly proportional to the irreversibility fraction of the domain wall nucleation process. Moreover, it gives more accurate values of this property than the remanence measured on the major hysteresis curve. During the same time, the irreversible switching field distribution increases abruptly, while the reversible one remains constant, information that is not possible to extract from the major hysteresis curve. In summary, the thin film uniaxial anisotropy influences predominantly the antidot array angular behaviour, through the irreversible part of the domain wall nucleation–propagation processes.

5. Conclusion

In conclusion, we have shown the ability of the physical analysis model applied to FORC results to easily probe the local magnetostatic properties of a nanometric FePd antidot array thin film with regular geometry, requiring only rather common magnetometric data. It yields to discriminate and quantify each magnetic process occurring during magnetization reversal. The accuracy of analysis depends on the correctness of the supposed magnetic behaviour, which can be simulated to test the initial hypotheses. In this study, despite the simplicity of the system used for the simulation, we succeeded in characterizing quantitatively both the reversible and the irreversible magnetization processes, linking each of them to a physical process and identifying

the surface roughness as the interaction field source. Therefore, it has been demonstrated that such a method can, in principle, be applied in other nanomagnetic systems, especially to probe the influence of one particular parameter on the system. Its main advantage is that it yields a complete description of the local magnetic behaviour, quantitatively describing each physical phenomenon. Also, it constitutes one of the few experimental ways of completely characterizing the magnetization reversal processes.

Acknowledgments

This work was financially supported in part by the *Fonds Québécois de Recherche sur la Nature et les Technologies* (FQRNT), Canada, the *Fundação de Amparo à Pesquisa do Estado de São Paulo* (FAPESP), Brazil, and the Spanish Government MICINN and EU FEDER under research projects nos MAT2009-13108-C02-01, MAT2010-20798-C05-04 and FICYT No FC-09-IB09-131. Small-angle x-ray scattering data was acquired at beamline D11A-SAXS1 at Laboratorio Nacional de Luz Sincroton (LNLS). We acknowledge Professor Cotta (UNICAMP) for the AFM measurements. MK acknowledges the Brazilian agency CNPq and the John Simon Guggenheim Memorial Foundation for the Guggenheim Fellowship 2009–2010.

References

[1] Barnard J A, Fujiwara H, Inturi V R, Jarratt J D, Scharf T W and Westona J L 1996 *Appl. Phys. Lett.* **69** 2758
[2] Tripathy D, Vavassori P, Porro J M, Adeyeye A O and Singh N 2010 *Appl. Phys. Lett.* **97** 042512
[3] Ruiz-Feal I *et al* 2002 *J. Magn. Magn. Mater.* **242–245** 597
[4] Vavassori P, Gubbiotti G, Zangani G, Yu C T, Yin H, Jiang H and Mankey G J 2002 *J. Appl. Phys.* **91** 7992
[5] Heyderman L J *et al* 2006 *Phys. Rev.* B **73** 214429
[6] Brigneti V, Ramos C A, Bermúdez Ureña E, Pirota K, Vázquez M, Prieto P and Sanz J M 2008 *J. Magn. Magn. Mater.* **320** e257
[7] Cowburn R P, Adeyeye A O and Bland J A C 1997 *Appl. Phys. Lett.* **70** 2309
[8] Vélez M, Martín J I, Villegas J E, Hoffmann A, González E M, Vicent J L and Schuller I K 2008 *J. Magn. Magn. Mater.* **320** 2547
[9] Vinckx W, Vanacken J, Moshchalkov V V, Mátéfi-Tempfli S, Mátéfi-Tempfli M, Michotte S and Piraux L 2006 *Eur. Phys. J.* B **53** 199
[10] Ctistis G, Papaioannou E, Patoka P, Gutek J, Fumagalli P and Giersig M 2009 *Nano Lett.* **9** 1
[11] Neusser S and Grundler D 2009 *Adv. Mater.* **21** 2927
[12] Barman A 2010 *J. Phys. D: Appl. Phys.* **43** 195002
[13] Mayergoyz I D 1986 *Phys. Rev. Lett.* **56** 1518
[14] Pike C R and Fernandez A 1999 *J. Appl. Phys.* **85** 6668
[15] Dumas R K, Li C P, Roshchin I V, Schuller I K and Liu K 2007 *Phys. Rev.* B **75** 134405
[16] Pike C R, Ross C A, Scalettar R T and Zimanyi G 2005 *Phys. Rev.* B **71** 134407
[17] Spinu L, Stancu A, Radu C, Li F and Wiley J B 2004 *IEEE Trans. Magn.* **40** 2116
[18] Béron F, Clime L, Ciureanu M, Ménard D, Cochrane R W and Yelon A 2008 *J. Nanosci. Nanotechnol.* **8** 2944
[19] Béron F, Carignan L-P, Ménard D and Yelon A 2008 *IEEE Trans. Magn.* **44** 2745
[20] Béron F, Carignan L-P, Ménard D and Yelon A 2010 *Electrodeposited Nanowires and their Applications* ed N Lupu (Vienna: IN-TECH) pp 167–88 http://www.intechopen.com/articles/show/title/extracting-individual-properties-from-global-behaviour-first-order-reversal-curve-method-applied-to- ISBN 978-953-7619-88-6
[21] Rahman M T, Dumas R K, Eibagi N, Shams N N, Wu Y-C, Liu K and Lai C-H 2009 *Appl. Phys. Lett.* **94** 042507

[22] Preisach F 1935 *Z. Phys.* **94** 277
[23] Béron F, Ménard D and Yelon A 2008 *J. Appl. Phys.* **103** 07D908
[24] Béron F, Clime L, Ciureanu M, Cochrane R W, Ménard D and Yelon A 2007 *J. Appl. Phys.* **101** 09J107
[25] Tejedor M and Fernández A 1986 *J. Magn. Magn. Mater.* **59** 28
[26] López-Antón R, Vega V, Prida V M, Fernández A, Pirota K R and Vázquez M 2009 *Solid State Phenom.* **152–153** 273
[27] Masuda H and Kukuda K 1995 *Science* **268** 1466
[28] Prida V M, Pirota K R, Navas D, Asenjo A, Hernández-Vélez M and Vázquez M 2007 *J. Nanosci. Nanotechnol.* **7** 272
[29] Kühnemund L, Edler T, Kock I, Seibt M and Mayr S G 2009 *New J. Phys.* **11** 113054
[30] Stancu A, Pike C, Stoleriu L, Postolache P and Cimpoesu D 2003 *J. Appl. Phys.* **93** 6620